Pathogenic tau does not drive activation of the unfolded protein response

Aleksandra P. Pitera[1], Ayodeji A. Asuni[2], Vincent O'Connor[1] and Katrin Deinhardt[1*]

Running title: *UPR is not induced in tauopathy*

[1]Biological Sciences, University of Southampton, UK
[2]Systems Biology - Symptoms, H. Lundbeck A/S, Denmark
* To whom correspondence should be addressed: K.Deinhardt@soton.ac.uk

Keywords: neuron, tau, tauopathy, transgenic mice, unfolded protein response (UPR), neurodegenerative disease, protein misfolding, frontotemporal dementia, primary hippocampal neuron

---

ABSTRACT

The unfolded protein response (UPR) is commonly associated with a range of neurodegenerative diseases, and targeting UPR components has been suggested as a therapeutic strategy. The UPR surveys protein folding within the endoplasmic reticulum (ER). However, many of the misfolded proteins that accumulate in neurodegeneration are localized such that they do not directly cause ER triggers that activate this pathway. Here, using a transgenic mouse model and primary cell cultures, along with qPCR, immunoblotting and immunohistochemistry, we tested whether UPR is induced in *in vivo* and *in vitro* murine models of tauopathy that are based on expression of mutant tau^{P301L}. We found no evidence for UPR in the rTg4510 mouse model in which mutant tau is transgenically expressed under control of tetracycline-controlled transactivator protein (tTA). This observation was supported by results from acute experiments in which neuronal cultures expressed mutant tau and accumulated misfolded cytoplasmic tau aggregates, but exhibited no UPR activation. These results suggest that the UPR is not induced as a response to tau misfolding and aggregation, despite clear evidence for progressive cellular dysfunction and degeneration. We propose that caution is needed when evaluating the implied significance of the UPR as a critical determinant across major neurodegenerative diseases.

Introduction

One of the common features of many neurodegenerative diseases is the presence of misfolded proteins that aggregate and disturb cellular homeostasis (1, 2). In order to prevent the consequences of misfolded protein aggregation, cells activate protective mechanisms such as the unfolded protein response (UPR) (2), however, chronic activation of the UPR is suggested to directly lead to pathology (2). UPR is induced upon the appearance of unfolded/misfolded proteins within the endoplasmic reticulum (ER). Its activation has been reported in Alzheimer's disease (AD), Parkinson's disease (PD) and Amyotrophic lateral sclerosis (ALS) (4, 5, 6). However, in these diseases the misfolded aggregates are mainly cytoplasmic or extracellular. Thus the misfolding pathway is independent of the ER lumen where the key triggers for the UPR are localised (6). While it remains a possibility that indirect activation of the ER-based UPR may occur (7), it is unclear how the disturbed cytoplasmic proteostasis associated with neurodegeneration couples to an UPR.

There are three branches of the UPR: inositol requiring enzyme-1 (IRE1), protein kinase R-like endoplasmic reticulum kinase (PERK) and

activating transcription factor 6 (ATF6), and together they aim to increase the protein folding capacity of the ER, decrease the global protein synthesis and stimulate the ER-associated degradation (8). Activation of all three cascades leads to the increased expression of the ER-resident chaperone BiP and to other events including splicing of the transcription factor XBP-1 and phosphorylation of the translation factor eIF2α that leads to the inhibition of mRNA translation (1). All those measures aim to alleviate misfolding-induced stress and if they fail, it can result in the dysfunction and eventually death of the cell (2).

A well-characterised model of neurodegeneration associated with the accumulation of dysfunctional protein is the rTg4510 mouse model of tauopathy, in which mice express tau^{P301L}, one of the most common human tau mutations underpinning frontotemporal dementia (9). As they age the rTg4510 mice show behavioural changes, cytosolic accumulation of neurofibrillary tangles (NFT) and atrophy of the forebrain (10, 11). The well-characterised progressive nature of the pathology enables sampling of tissues from distinct phases of the disease, allowing molecular investigation of the accumulating dysfunction.

In this study, we used the rTg4510 mice to investigate the mechanisms underlying UPR activation in response to a cytosolic protein aggregation, but found no evidence for tau-triggered UPR activation. rTg4510 mice are generated by crossing two lines of transgenic mice: one expressing the tetracycline-controlled transactivator protein (tTA) driven by the CaMKII promoter, and the second expressing the tetracycline-responsive promoter element (TRE) placed upstream of the cDNA encoding human tau^{P301L} (10). To distinguish the effects exerted by mutant tau from those that were driven by the expression of the transactivator protein, we compared the animals overexpressing human tau not only to wildtype mice but also to the mice carrying the tTA element.

To probe tau^{P301L}-dependent UPR induction in a more acute model with no confound resulting from transactivator expression, we investigated primary hippocampal neurons expressing human tau^{P301L}, which misfolds when expressed in primary neurons, or tau^{WT}. We found that while primary hippocampal neurons are capable of inducing UPR, they fail to do so in response to tau misfolding. Thus, our data indicate that pathogenic tau fails to mount an evidenced UPR in distinct models of chronic and acute tau-mediated dysfunction.

Results

rTg4510 mice are characterised by progressive neurodegeneration.

We benchmarked the tissue utilised to investigate UPR activation against the previously characterised disease progression in the rTg4510 mice (10, 11). The weight of the brains used in this study was decreased in 6- and 9-month-old mice when compared to the age-matched wild-type mice, with two-way ANOVA revealing an effect of age ($F_{(2, 19)}$=8.296 , p=0.0026), genotype ($F_{(2, 19)}$=59.7, p<0.0001) and the age-genotype interaction ($F_{(4, 19)}$=8.172, p=0.0005) on the brain weight (Figure 1A). The brain weight was also decreased in 3-month-old tTA mice compared to age-matched WT (p=0.0319). However, there was no further decrease of brain weight in the tTA mice over time, whereas the rTg4510 mice presented a progressive decrease. This is consistent with an observation made in a previous study (12) and highlights both a tTA-dependent effect and an additional and more protracted tau-mediated pathology. This alerted us to potential stress-related tTA effects independent of the tau dysfunction. To control for this, our study compared wildtype, tTA and tTA::tau^{P301L} transgenic cohorts.

We assessed the tau load in these cohorts by measuring the level of total and phosphorylated tau (Ser396/404) (Figure 1B, C). In accordance with previously published data (10) an increased level of tau was observed in the rTg4510 mice, whereas the expression and phosphorylation levels in tTA

and WT mice were comparable. Statistical analysis showed a genotype effect on the level of total tau ($F_{(2, 18)}$=19.17, p<0.0001) and phospho-tau ($F_{(2, 17)}$=16.1, p=0.0001). A slight decrease of total tau and a significant decrease of phospho-tau was observed between 6- and 9-month-old rTg4510 mice (p=0.0044). Therefore, we quantified the p-tau levels not only relative to GAPDH, but also relative to total tau. In both instances a decreased level of p-tau was observed at 9 months when compared to the level at 6 months. This observation had been made previously and had been ascribed to the progressive loss of neurons in rTg4510 mice, and in particular the loss of those neurons bearing a high tangle load (10).

The level of GFAP was also determined to investigate appearance of astrogliosis. The expression of this astrocytic marker was comparable between all the genotypes examined in 3-month-old mice. The level of GFAP was higher in 6-month-old rTg4510 mice and it was further increased at the later 9-month time point (Figure 1D). Two-way ANOVA revealed the effect of age ($F_{(2, 15)}$= 4.62, p=0.0273) and genotype ($F_{(2, 15)}$=7.089, p=0.0068) and also the age-genotype interaction ($F_{(4, 15)}$=3.4, p=0.0361) on the GFAP level. The increased GFAP level is a direct indication for increasing pathology and has been reported by others (13).

The transgene disrupts a range of forebrain structures, and here we examined the hippocampus, reported to be one of the most affected regions in rTg4510 model (10). The brain slices were stained with the neuronal marker, NeuN (Figure 1E, F). The staining revealed the progressive atrophy of the whole hippocampal formation, with the CA1 region being the most affected, confirming the previously published data (10, 12). Thinning of the dentate gyrus of tTA mice was also observed, which is in accordance with published observations (12).

Overall, these results confirm that our rTg4510 tissue displays the established features of progressive neurodegeneration that is accompanied by increased load of phosphorylated tau and by astrogliosis. Furthermore, it reveals the presence of tTA-dependent signalling that highlights the need for an additional control when probing the tissue from the rTg4510 mice for previously uninvestigated parameters.

The IRE1 and PERK branches are not activated in rTg4510 mice.

Next, we proceeded to investigate whether the IRE1 branch of UPR is induced in the hippocampus of rTg4510 mice. When activated, IRE1 leads to alternative splicing of the XBP-1 mRNA (Figure 2A), and the spliced form activates the transcription of genes that play a role in ER quality control (14). To verify whether the splicing event takes place in rTg4510 mice, the primers detecting both, spliced and unspliced forms were designed and their specificity was confirmed using tunicamycin-treated mouse embryonic fibroblasts (MEFs) (Figure 2B). Resolving the PCR products on the agarose gel revealed the presence of two bands, with the upper one corresponding to the unspliced form and the lower band, devoid of the 26 base pair intron, corresponding to the spliced variant of XBP-1. Both spliced and unspliced species were present in the tunicamycin-treated sample, with only one XBP-1 band, corresponding to the unspliced form, present in the vehicle-treated and untreated MEFs. This result confirms the ability of the primers to detect XBP-1 splicing. The primers were then used to verify whether the splicing occurs in the hippocampus of rTg4510 mice. We did not observe the band corresponding to the spliced form of XBP-1 at any of the time points investigated (Figure 2C).

To further investigate UPR activation in rTg4510 mice, we decided to determine the level of phosphorylated eukaryotic initiation factor 2α (eIF2α). Upon UPR activation, PERK phosphorylates eIF2α, that results in the inhibition of mRNA translation and alleviation of ER stress (15). The Western blot results showed no detectable p-PERK (Figure S1) and no increase of p-eIF2α in rTg4510 mice

(Figure 2D). Two-way ANOVA revealed the age effect ($F_{(2, 17)}$=5.016, p=0.0194) but failed to find a genotype effect ($F_{(2, 17)}$=0.04761, p=0.9536) or an age-genotype interaction ($F_{(4, 17)}$=1.457, p=0.2588). Together this suggests that the IRE1 and PERK branches of the UPR are not activated in the rTg4510 brains.

The expression level of shared UPR markers is not increased in rTg4510 mice.

To further examine the UPR in rTg4510 mice, we focused on BiP, an ER chaperone that is robustly transcribed in face of an UPR and that is involved in all three arms of the response. qPCR and Western blot techniques were used to determine mRNA and protein levels, respectively. The mRNA level was not different between rTg4510, WT and tTA mice (Figure 3A). Two-way ANOVA revealed an age effect ($F_{(2, 18)}$=3.656, p=0.0465) but no effect of the genotype ($F_{(2, 18)}$=1.357, p=0.2825) and no interaction ($F_{(4, 18)}$=1.266, p=0.3196) between age and genotype on the BiP mRNA level. The protein expression was significantly increased in 9-month-old rTg4510 mice when compared to 9-month-old WT mice (p=0.0351) (Figure 3B). However, there was no difference in the BiP protein level between tTA and rTg4510 mice (p=0.7004) suggesting that the increased BiP expression is not due to the presence of mutant human tau.

Finally, we focused on CHOP that is involved in UPR-induced cell death. Expression of CHOP can be induced by all three UPR branches (16), as well as by other stressors, including mitochondrial and oxidative stress (16). Similar to BiP, its mRNA and protein expression levels were determined using qPCR and Western blot, respectively. No changes at the transcript level were found at any of the time points investigated (Figure 3C). Two-way ANOVA failed to find an age effect ($F_{(2, 18)}$= 0.4137, p=0.6673), genotype effect ($F_{(2, 18)}$=0.1025, p=0.9031) or an age-genotype interaction ($F_{(4, 18)}$=1.832, p=0.1660). In contrast, statistical analysis of CHOP protein revealed the effect of both, age ($F_{(2, 15)}$=14.31, p=0.0003) and genotype ($F_{(2, 15)}$=11.21, p=0.0011) as well as the age-genotype interaction ($F_{(4, 15)}$=7.911, p=0.0012) (Figure 3D). Tukey's post hoc test further showed that CHOP level was increased in 9-month-old rTg4510 mice when compared to WT (p=0.0292), but not when compared to tTA mice (p=0.2115). Interestingly, significantly higher level of CHOP protein was also observed in 3-month-old tTA mice compared to age-matched WT (p<0.0001) or rTg4510 mice (p=0.0035). The observed late stage increase of CHOP protein occurs without accompanying changes in other UPR markers, suggesting that it may not be related to an ER stress. Thus, we find no compelling evidence for UPR activation across key stages of the time course that encompasses the progressive pathologies expressed in the rTg4510 model of tauopathy.

Primary neurons are susceptible to UPR.

The lack of UPR activation in the model of progressive tauopathy may suggest that hippocampal neurons are not prone to undergoing UPR activation. To test that hypothesis, primary hippocampal neurons were treated with tunicamycin for 6 or 24 hours. MEF cells that are able to activate UPR were treated with tunicamycin as a positive control. The increase in BiP expression in hippocampal neurons was seen after a 6 h treatment and it remained upregulated at the 24 h time point (Figure 4A). Similarly, the induction of CHOP mRNA level was detected already after 6 h treatment (Figure 4B).

To further confirm the ability of neurons to undergo UPR, RNA was extracted from primary neurons treated with tunicamycin for 6 or 24 h, and the splicing of XBP-1 was examined. The IRE-1 branch of UPR was activated already after 6 h treatment – two bands corresponding to unspliced and spliced form of XBP-1 were present in both, 6 and 24 h treatment conditions (Figure 4C).

These results indicate that harsh treatment, such as applying a glycosylation inhibitor, leads to the activation of UPR in primary neurons, thereby showing the susceptibility of neurons to this response.

Expressing tauP301L in primary neurons does not result in UPR activation.

Having found that neurons are able to induce the UPR, we next examined whether misfolding of tau in cultured hippocampal neurons can drive UPR activation. This approach allows us to isolate the effects triggered by pathogenic tau^{P301L} and eliminate confounds resulting from tTA expression, which are particularly pronounced at the early time points we investigated in the Tg4510 model. Expression of RFP-tau^{P301L} in hippocampal neurons results in the presence of red fluorescent aggregates along the axon that are not observed in RFP-tau^{WT} expressing neurons (Figure 5A). Immunostaining with the conformation-specific antibody MC-1 (17) confirmed that these aggregates report misfolded tau. Importantly, MC-1 staining was observed only in tau^{P301L}-transfected cells, whereas no immunoreactivity could be detected for tau^{WT}-transfected neurons (Figure 5A). Thus, this approach can be used to verify if misfolded tau and associated dysfunctional proteostasis drives UPR activation.

At day in vitro (DIV) 14, no XBP-1 splicing was observed in the tau^{P301L}- or tau^{WT}-electroporated cells (Figure 5B), whereas both bands were present in the tunicamycin-treated MEFs. To examine the expression of other UPR markers, qPCR experiments for BiP and CHOP were performed. Neither of the genes was significantly different between neurons electroporated with tau^{P301L} and tau^{WT} (t-test, p=0.3360 and p=0.3698, respectively) (Figure 5C, D), regardless whether the expression was normalised to a housekeeping gene or to the independently quantified expression of exogenous human tau. These results suggest that the presence of mutated and misfolded tau does not lead to the induction of UPR.

Discussion

Here, we tested whether the UPR is activated by the presence of misfolded tau. We tested both a mouse model of tauopathy as well as primary hippocampal neurons *in vitro*. This gave us traction to investigate the phenomenon in two distinct but complimentary systems.

The UPR is a homeostatic mechanism that can become dysregulated and has been discussed as a significant driver of pathology across many neurodegenerative diseases. This concept has been reinforced by preclinical studies that show that targeting arms of the UPR with inhibitors has therapeutic potential (18–20). Tau is one of the proteins whose aggregation is found in neurodegenerative diseases, and it has been reported that presence of misfolded tau can induce the UPR (18, 20). However, it raises an important question of how the cytosolic aggregates of tau protein, which do not enter the ER lumen, can induce a response designed to counteract protein misfolding within the ER lumen. As UPR activation has been previously demonstrated in the rTg4510 model of tauopathy (18, 20, 21), we decided to use this model to explore how a cytosolic misfolding triggers an ER luminal response.

We tested four commonly used markers of the UPR: XBP-1, p-eIF2α, BiP and CHOP and found no indication that the UPR is activated in rTg4510 mice. A significant change for rTg4510 compared to wildtype mice was observed for BiP protein in 9-month-old mice, but an increase was also observed in mice expressing the activator transgene tTA alone, suggesting that the change is not driven by mutant tau expression. A tTA-induced effect can also be seen for CHOP protein levels in 3-month-old mice, which display significantly increased levels when compared to WT and rTg4510 mice. This suggests that the neurons that develop in the face of the tTA transgene are not indifferent to its expression. Indeed, tTA expression in mice has been associated with a range of changes including reduction in the number of dentate granule neurons and alterations in gene expression (12, 22).

The rTg4510 model has been previously used to investigate UPR activation. Radford et al. observed no splicing of XBP-1, suggesting the lack of activation of IRE-1 pathway, which is consistent with our data (18). However, the increased level of other UPR markers,

including p-eIF2α and p-PERK, was observed in other studies where WT mice were compared to rTg4510 mice (18, 20). We could not see a difference in the level of phosphorylated eIF2α in our samples using the antibody directed against the same phospho-epitope (Ser51) as the one in the studies of Radford et al. and Halliday et al. We further were unable to detect p-PERK in the rTg4510 samples (Figure S1), and thus found no evidence for an activation of the PERK branch of the UPR in response to tau pathology *in vivo*.

To further investigate UPR activation as a response to tau misfolding, we used an *in vitro* approach where we transfected primary neurons with tau^{P301L} or tau^{WT}. In this system we observed tau misfolding upon mutant tau expression, suggesting that it can be used to model tau pathology. Exogenously expressed RFP-tau appeared cytosolic or microtubule-associated in nature, with no reticulate pattern observed (data not shown). The culture approach allows us to isolate the effects of tau^{P301L} expression from those of tTA expression. Comparing tau^{WT} and tau^{P301L}-electroporated cells revealed no difference in the expression of UPR markers. This further suggests that the upregulation of UPR components observed in the rTg4510 mice is due to the presence of the tTA component as opposed to the accumulation of mutated tau.

Similar observations concerning the lack of UPR activation by mutant tau had been made when using HEK293 cells expressing tau^{P301L}, with tau expression controlled by tetracycline-regulated T-Rex expression system. Neither splicing of XBP-1 nor induction of protein markers of the UPR had been observed in this system upon the overexpression of recombinant tau (23).

Our results highlight the need to carefully control any data obtained from transgenic models based on the tetracycline transactivator system. The tTA system contains DNA- and tetracycline-binding domains of *E. coli* tetracycline repressor and the transcriptional activation domain of the herpes simplex virion protein 16 (24). This latter component likely interacts with endogenous transcription factors leading to the changes observed for tTA expressing mice. It has for example been shown that the presence of the tTA transgene leads to alterations in the gene expression in myocardium. Among the changing genes were those involved in metabolism and those encoding different chaperones (25). Large differences in gene expression between brains from WT and tTA mice have also been reported (22).

It has previously been questioned whether UPR activation occurs in neurodegenerative models: Hashimoto et al. detected no UPR induction in APP knock-in mice, single APP-overexpressing mice and a distinct model of tauopathy: the P301S Tau-Tg mice (26). They suggested that the UPR activation observed for different transgenic models may be an artefact resulting from the expression of membrane proteins that could generate a non-specific ER stress. The lack of UPR activation in the tauopathy model could be explained by the cytosolic localisation of tau protein, with no indication of tau entering the ER lumen (26).

On the other hand, other studies have reported neuroprotective effects in the rTg4510 mice following treatment with GSK2606414. This drug was used on the basis that it acts as an inhibitor of PERK, and its inhibition would execute its effect by interfering with the UPR. The treatment decreased levels of tau phosphorylation, reduced brain atrophy and prevented behavioural scores of dysfunction (18). Of note, the inhibitor used in the cited study is not PERK-selective. It has been shown that it can potently inhibit Receptor-interacting serine/threonine-protein kinase 1 (27). Therefore, the impressive improvement of the rTg4510 mice in response to GSK2606414 treatment may be a result of inhibiting necroptosis rather than the UPR.

Conflicting results have been reported for human cases of AD. BiP levels have been reported to be increased, decreased, or not changed between AD and control brains by different research groups (27, 28, 29). Hoozemans et al. reported increased BiP expression using Western blot and immunohistochemistry, whereas Sato et al. did

not detect an increase between control and familial or sporadic cases of AD (28, 29). Katayama et al. observed decreased levels of BiP in both sporadic and familial AD cases when compared to non-demented controls (30). Lee et al. reported an increase in XBP-1 splicing in AD cases, however they observed the spliced form of the gene in the control brains as well, suggesting that the splicing event is not a disease-specific feature (31), and we have seen similar variation between AD and age matched non-demented cohort (unpublished observation) highlighting the intrinsic difficulty of quantifying such stress pathways in pathological tissue (26).

In conclusion, while there is good evidence for UPR activation in some neurodegenerative diseases, its causative role across neurodegeneration is less clear, particularly in view of the neurodegeneration-independent activation of UPR observed in some of the mouse models.

Experimental procedures

Materials

Primary antibodies used in this study are: anti-actin (Sigma AC-40), anti-BiP (Cell Signaling, 3177), anti-CHOP (Cell Signaling, 2896), anti-p-eIF2α (Cell Signaling, 3398), anti-eIF2α (Cell Signalling, 9722), anti-tau (DAKO, A0024), anti-GFAP (DAKO, Z0334), anti-NeuN (Cell Signaling, 12943), anti-GAPDH (Abcam, ab8245), MC-1 and PHF-1 (gifts from Prof. Peter Davies) (17). Secondary antibodies were conjugated to AlexaFluor fluorophores (Invitrogen) or IRDyes (LiCOR).

The plasmids pRK5-EGFP-TauP301L and pRK5-EGFP-Tau were gifts from Karen Ashe (Addgene plasmids no. 46908 and 46904, respectively) (32), and GFP in the constructs was exchanged for RFP.

Primers were obtained from Eurofins Genomics. BiP: 5-ATTGGAGGTGGGCAAACCAA-3 (forward), 5-TCGCTGGGCATCATTGAAGT-3 (reverse); CHOP: 5-TCCCCAGGAAACGAAGAGGAAG-3 (forward), 5-TCATGCGTTGCTTCCCAGGC-3 (reverse); XBP-1: 5-GGAGTGGAGTAAGGCTGGTG-3 (forward), 5-GTCCAGAATGCCCAAAAGGATA-3 (reverse).

Primers for the reference gene, eIF4a were purchased from Primer Design.

Mice

rTg4510 and age-matched wild-type and tTA mice were provided by Lundbeck (Denmark). Mice were euthanized by cervical dislocation, and the brains were quickly removed and portioned. One hemisphere was immersion-fixed in 4% paraformaldehyde for 36 hours and processed for histology. While the other hemisphere was snap-frozen on dry ice and stored at –80°C until use. All rTg4510 experiments were performed in accordance with the European Communities Council Directive #86/609, the directives of the Danish National Committee on Animal Research Ethics, and Danish legislation on experimental animals.

For tissue collection, C57Bl/6 wildtype mice were sacrificed in accordance with the Animals (Scientific Procedures) Act 1986 as approved by the UK home office.

Cell culture

Primary neurons were prepared in Dulbecco's PBS (Life Technologies) from hippocampi of E15-E18 C57Bl/6 mice. Neurons were dissociated as described (33). The number of cells was determined and the cells were either plated or subjected to electroporation.

Electroporation was performed using Mouse Neuron Nucleofector® Kit (Lonza) according to the manufacturer's instructions. After the electroporation procedure, neurons were incubated in the recovery medium containing complete NBM (Neurobasal medium with 2% B27 supplement and 0.5 mM Glutamax) with additional 10% FBS at 37°C for 45 minutes. The electroporated cells were resuspended in NBM and plated. The electroporation efficiency was consistently around 70-80%.

Mouse embryonic fibroblasts (MEFs) were isolated from E15 C57Bl/6 mice and maintained in D-MEM with 10% FBS.
For tunicamycin treatment, the cells were treated with tunicamycin (2 µg/ml, Abcam) or 0.1% DMSO (vehicle treatment) prepared in media. The cells were incubated in 37°C for 6 or 24 hours and then harvested.

Immunocytochemistry
Cells were transfected at 1 day in vitro (DIV) with Lipofectamine 2000 as described (30). The lipoplex mix was added to the cells and incubated at 37°C for 40 minutes. Subsequently, the lipoplex containing media was removed from the wells and replaced with the conditioned media, the cells were returned to the 37°C.
At day 14 in vitro, the cells were fixed and stained with MC-1 antibody (1:300). AlexaFluor 488 was used as a secondary antibody. Hoechst stain was used to stain the nuclei.
The cells were imaged using a 60x/1.42NA Oil Plan APO objective on a DeltaVision Elite system (GE Life Sciences) with an SSI 7-band LED for illumination and a monochrome sCMOS camera, using SoftWoRks software (version 6). DAPI/FITC/TRITC channels were used. The images were analysed using Fiji processing package (34).

Immunohistochemistry
Mice were perfused using 0.9% saline and then 4% paraformaldehyde (PFA). The mouse brains were fixed in 4% PFA for 48 h and then in 30% sucrose for 48 h. A microtome was used to cut 30 µm -thick coronal sections. The sections were permeabilized in blocking solution (TBS containing 10% normal goat serum (Invitrogen), 2% BSA and 0.4% Triton X-100, both from Fisher Scientific) at room temperature for 2 h. Next, the sections were incubated in the blocking solution containing NeuN antibody (1:500) overnight at 4°C. The incubation with primary antibody was followed by the incubation with the blocking solution containing Alexa Fluor-555 secondary antibody (Life Technologies, 1:500) for 2 h at room temperature. Before mounting the brain sections onto glass, sections were incubated in PBS containing Hoechst stain (1:10000, Invitrogen) for 10 minutes.
Overview images were acquired using a Nikon Eclipse E800 microscope using 4x/0.2 NA Plan Apo objective with an Optimus sCMOS camera. DAPI/TRITC channels were used to take images. Images of the CA1 region were acquired using a Leica SP8 scanning confocal microscope using 40x/1.30NA HC PI Apo CS2 oil immersion objective with a PCO Edge 5.5 sCMOS camera. Wave solid state lasers at 405 and 561 nm were used for illumination. The images were analysed using Fiji software (34).

Tissue homogenization
The hippocampi and cortici from wild-type, tTA, rTg4510 mice were homogenized in sterile PBS containing cOmplete Mini EDTA-free Protease Inhibitor Cocktail tablets (Roche), sodium fluoride (10 mM, Fisher Scientific) and sodium orthovanadate (2 mM). The samples were homogenized using Kontes pellet pestle motor and plastic pellet pestles. The samples homogenized in PBS were then used for RNA or protein extraction (35).

qPCR
RNA was isolated from the hippocampi of wild-type, tTA, rTg4510 mice using the Trizol method. The RNA was then purified using RNeasy kit (Qiagen). RNA from the cells was isolated and purified using RNeasy kit. RNA extracted from the hippocampi and cells was reverse transcribed using Precision nanoScript 2 reverse transcription kit (Primer Design) according to manufacturer's instructions.
qPCR was performed using Precision PLUS Mastermix (Primer Design) according to the manufacturer's instructions. The primers specific for detection of mouse BiP and CHOP were used to detect the respective mRNA levels. qPCR was performed using StepOnePlus Real-Time PCR instrument (Applied Biosystems) using the following conditions: hot start 95°C for 2 min and 40

cycles of denaturation at 95°C for 10 s and data collection at 60°C for 1 min.
All reactions were performed with two technical replicates. The expression level was normalized to the level of the reference gene, eIF4a.

XBP-1splicing
End point PCR using RedTaq ReadyMix PCR Reaction Mix (Sigma Aldrich) and the primers detecting both, spliced and unspliced, forms of XBP-1 were used. PCR was performed using GeneAmp PCR System 9700 (Applied Biosystems) and the following conditions were used: hot start at 94°C for 2 min, 40 cycles of: denaturation at 94°C for 40 s, annealing at 60°C for 30 s, extension at 72°C for 1 min. Then the final extension was performed at 72°C for 10 min. The products of PCR reaction were separated on 2.5% agarose gel.

Western blotting
The proteins were extracted from the PBS-homogenised hippocampi and cortici using 2x homogenization buffer containing HEPES-NaOH (40 mM, pH 7.4, Fisher Scientific), NaCl (250 mM, Sigma Aldrich), SDS (4%), cOmplete Mini EDTS-free Protease Inhibitor Cocktail tablets (Roche), sodium fluoride (10 mM) and sodium orthovanadate (2 mM). The samples were mixed with 5x sample buffer containing tris (312.5 mM, pH 6.8, SDS (10%), glycerol (50%), dithiothreitol (25 mM) and bromophenol blue dye (0.005%).
The cells were lysed in the 2x sample buffer containing Tris-HCl (125 mM, pH 6.8), SDS (4%), glycerol (20%), dithiothreitol (10 mM) and bromophenol blue dye (0.002%),
The samples were boiled for 10 min at 95°C, spun and then separated by SDS-PAGE and transferred to nitrocellulose membrane. The membranes were blocked in 2.5% BSA, TBS-T for 1h and then incubated at 4°C overnight with the primary antibody. The membrane was then incubated with the secondary antibody at room temperature for 1 h. Images were captured using an Odyssey Infrared Imaging System (LI-COR Biosciences). The Image Studio Scanner software was used to obtain the image and Image Studio Lite software was used to quantify the intensities of the bands.

Acknowledgements
We thank Johanna Penfold and Dr Matthew Davies for providing a positive control for p-eIF2A blotting. This work was funded by Alzheimer's Society with support from the Healthcare Management Trust (AS-PhD-2015-029, APP).

Conflict of interest: APP, VOC and KD declare that they have no conflict of interest. AAA is a full-time employee of H. Lundbeck A/S, Denmark.

Author contributions: KD and VOC conceptualised the study. APP, KD and VOC designed experiments and analysed the data. APP performed the experiments. AAA provided the transgenic tissue and advised on the mouse strain. APP, AAA, KD and VOC wrote the manuscript.

1. Roussel, B. D., Kruppa, A. J., Miranda, E., Crowther, D. C., Lomas, D. A., and Marciniak, S. J. (2013) Endoplasmic reticulum dysfunction in neurological disease. *Lancet Neurol.* **12**, 105–118
2. Forman, M. S., Lee, V. M. Y., and Trojanowski, J. Q. (2003) "Unfolding" pathways in neurodegenerative disease. *Trends Neurosci.* **26**, 407–410
3. Hoozemans, J. J. M., Van Haastert, E. S., Nijholt, D. A. T., Rozemuller, A. J. M., Eikelenboom, P., and Scheper, W. (2009) The Unfolded Protein Response Is Activated in Pretangle Neurons in Alzheimer's Disease Hippocampus. *Am. J. Pathol.* **174**, 1241–1251
4. Hoozemans, J. J. M., van Haastert, E. S., Eikelenboom, P., de Vos, R. A. I., Rozemuller, A. J. M., and Scheper, W. (2007) Activation of the unfolded protein response in Parkinson's disease. *Biochem. Biophys. Res. Commun.* **354**, 707–711
5. Ilieva, E. V., Ayala, V., Jové, M., Dalfó, E., Cacabelos, D., Povedano, M., Bellmunt, M. J., Ferrer, I., Pamplona, R., and Portero-Otín, M. (2007) Oxidative and endoplasmic reticulum stress interplay in sporadic amyotrophic lateral sclerosis. *Brain*. **130**, 3111–3123
6. Smith, H. L., and Mallucci, G. R. (2016) The unfolded protein response: Mechanisms and therapy of neurodegeneration. *Brain*. **139**, 2113–2121
7. Liu, X. De, Ko, S., Xu, Y., Fattah, E. A., Xiang, Q., Jagannath, C., Ishii, T., Komatsu, M., and Eissa, N. T. (2012) Transient aggregation of ubiquitinated proteins is a cytosolic unfolded protein response to inflammation and endoplasmic reticulum stress. *J. Biol. Chem.* **287**, 19687–19698
8. Cao, S. S., and Kaufman, R. J. (2012) Unfolded protein response. *Curr. Biol.* **22**, R622–R626
9. Tacik, P., Sanchez-Contreras, M., DeTure, M., Murray, M. E., Rademakers, R., Ross, O. A., Wszolek, Z. K., Parisi, J. E., Knopman, D. S., Petersen, R. C., and Dickson, D. W. (2017) Clinicopathologic heterogeneity in FTDP-17 due to MAPT p.P301L mutation, including a patient with globular glial tauopathy. *Neuropathol Appl Neurobiol.* **43**, 200–214
10. Ramsden, M., Kotilinek, L., Forster, C., Paulson, J., McGowan, E., SantaCruz, K., Guimaraes, A., Yue, M., Lewis, J., Carlson, G., Hutton, M., and Ashe, K. (2005) Age-Dependent Neurofibrillary Tangle Formation, Neuron Loss, and Memory Impairment in a Mouse Model of Human Tauopathy (P301L). *J. Neurosci.* **25**, 10637–10647
11. SantaCruz, K. (2005) Tau Suppression in a Neurodegenerative Mouse Model Improves Memory Function. *Science (80-.).* **309**, 476–481
12. Helboe, L., Egebjerg, J., Barkholt, P., and Volbracht, C. (2017) Early depletion of CA1 neurons and late neurodegeneration in a mouse tauopathy model. *Brain Res.* **1665**, 22–35
13. Blair, L. J., Frauen, H. D., Zhang, B., Nordhues, B. A., Bijan, S., Lin, Y., Zamudio, F., Hernandez, L. D., Sabbagh, J. J., Selenica, M. B., and Dickey, C. A. (2015) Tau depletion prevents progressive blood-brain barrier damage in a mouse model of tauopathy. 10.1186/s40478-015-0186-2
14. Chen, Y., and Brandizzi, F. (2014) IRE1: ER stress sensor and cell fate executor. *Trends Cell Biol.* **23**, 22–25
15. Walter, P., and Ron, D. (2011) the Unfolded Protein Response : From Stress Pathway to Homeostatic Regulation. *Science (80-.).* **334**, 1081–1086
16. Oyadomari, S., and Mori, M. (2004) Roles of CHOP / GADD153 in endoplasmic reticulum stress. 10.1038/sj.cdd.4401373
17. Jicha, G. A., Bowser, R., Kazam, I. G., and Davies, P. (1997) Alz-50 and MC-1, a new monoclonal antibody raised to paired helical filaments, recognize conformational epitopes

on recombinant tau. *J. Neurosci. Res.* **48**, 128–132
18. Radford, H., Moreno, J. A., Verity, N., Halliday, M., and Mallucci, G. R. (2015) PERK inhibition prevents tau-mediated neurodegeneration in a mouse model of frontotemporal dementia. *Acta Neuropathol.* **130**, 633–642
19. Moreno, J. A., Radford, H., Peretti, D., Steinert, J. R., Verity, N., Martin, M. G., Halliday, M., Morgan, J., Dinsdale, D., Catherine, A., Barrett, D. A., Tsaytler, P., Bertolotti, A., Willis, A. E., and Mallucci, G. R. (2012) Sustained translational repression by eIF2a – P mediates prion neurodegeneration. **485**, 507–511
20. Halliday, M., Radford, H., Zents, K. A. M., Molloy, C., Moreno, J. A., Verity, N. C., Smith, E., Ortori, C. A., Barrett, D. A., Bushell, M., and Mallucci, G. R. (2017) Repurposed drugs targeting eIF2 a -P-mediated translational repression prevent neurodegeneration in mice. *Brain*. 10.1093/brain/awx074
21. Abisambra, J. F., Jinwal, U. K., Blair, L. J., Iii, J. C. O. L., Li, Q., Brady, S., Wang, L., Guidi, C. E., Zhang, B., Nordhues, B. A., Suntharalingham, A., Li, P., Jin, Y., and Atkins, C. A. (2013) Tau accumulation activates the unfolded protein response by impairing endoplasmic reticulum-associated degradation. **33**, 9498–9507
22. Wes, P. D., Easton, A., Corradi, J., Barten, D. M., Devidze, N., Decarr, L. B., Truong, A., He, A., Barrezueta, N. X., Polson, C., Bourin, C., Flynn, M. E., Keenan, S., Lidge, R., Meredith, J., Natale, J., Sankaranarayanan, S., Cadelina, G. W., Albright, C. F., and Cacace, A. M. (2014) Tau Overexpression Impacts a Neuroinflammation Gene Expression Network Perturbed in Alzheimer ' s Disease. **9**, 24–31
23. Spatara, M. L., and Robinson, A. S. (2010) Transgenic Mouse and Cell Culture Models Demonstrate a Lack of Mechanistic Connection Between Endoplasmic Reticulum Stress and Tau Dysfunction. **88**, 1951–1961
24. Han, H. J., Allen, C. C., Buchovecky, C. M., Yetman, M. J., Born, A., Marin, M. A., Rodgers, S. P., Song, B. J., and Lu, H. (2013) Strain background influences neurotoxicity and behavioral abnormalities in mice expressing the tetracycline transactivator Harry. **32**, 10574–10586
25. McCloskey, D. T., Turnbull, L., Swigart, P. M., Zambon, A. C., Turcato, S., Joho, S., Grossman, W., Conklin, B. R., Simpson, P. C., and Baker, A. J. (2005) Cardiac transgenesis with the tetracycline transactivator changes myocardial function and gene expression. *Physiol Genomics*. **22**, 118–26
26. Hashimoto, S., Ishii, A., Kamano, N., Watamura, N., Saito, T., Oshima, T., Yokosuka, M., and Saido, T. C. (2018) Endoplasmic reticulum stress responses in mouse models of Alzheimer disease: overexpression paradigm versus knock-in paradigm. *J. Biol. Chem.* 10.1074/jbc.M117.811315
27. Rojas-Rivera, D., Delvaeye, T., Roelandt, R., Nerinckx, W., Augustyns, K., Vandenabeele, P., and Bertrand, M. J. M. (2017) When PERK inhibitors turn out to be new potent RIPK1 inhibitors: Critical issues on the specificity and use of GSK2606414 and GSK2656157. *Cell Death Differ.* **24**, 1100–1110
28. Hoozemans J. J. M., Veerhuis R., Van Haastert E. S., Rozemuller J. M., Baas F., Eikelenboom P., S. W. (2005) The unfolded protein response is activated in Alzheimer ' s disease. 10.1007/s00401-005-1038-0
29. Sato, N., Urano, F., Yoon Leem, J., Kim, S. H., Li, M., Donoviel, D., Bernstein, A., Lee, A. S., Ron, D., Veselits, M. L., Sisodia, S. S., and Thinakaran, G. (2000) Upregulation of BiP and CHOP by the unfolded-protein response independent of presenilin expression. *Nat. Cell Biol.* **2**, 863–870
30. Katayama, T., Imaizumi, K., Sato, N., Miyoshi, K., Kudo, T., Hitomi, J., Morihara, T., Yoneda, T., Gomi, F., Mori, Y., Nakano, Y., Takeda, J., Tsuda, T., Itoyama, Y.,

Murayama, O., Takashima, a, St George-Hyslop, P., Takeda, M., and Tohyama, M. (1999) Presenilin-1 mutations downregulate the signalling pathway of the unfolded-protein response. *Nat. Cell Biol.* **1**, 479–485

31. Lee, J. H., Won, S. M., Suh, J., Son, S. J., Moon, G. J., Park, U. J., and Gwag, B. J. (2010) Induction of the unfolded protein response and cell death pathway in alzheimer's disease, but not in aged Tg2576 mice. *Exp. Mol. Med.* **42**, 386–394
32. Hoover, B. R., Reed, M. N., Su, J., Penrod, R. D., Kotilinek, L. A., Grant, M. K., Pitstick, R., Carlson, G. A., Lanier, L. M., Yuan, L. L., Ashe, K. H., and Liao, D. (2010) Tau Mislocalization to Dendritic Spines Mediates Synaptic Dysfunction Independently of Neurodegeneration. *Neuron*. **68**, 1067–1081
33. Deinhardt, K., Kim, T., Spellman, D. S., Mains, R. E., Eipper, B. A., Neubert, T. A., Chao, M. V., and Hempstead, B. L. (2011) Neuronal growth cone retraction relies on proneurotrophin receptor signaling through rac. *Sci. Signal.* 10.1126/scisignal.2002060
34. Schindelin, J., Arganda-Carreras, I., Frise, E., Kaynig, V., Longair, M., Pietzsch, T., Preibisch, S., Rueden, C., Saalfeld, S., Schmid, B., Tinevez, J. Y., White, D. J., Hartenstein, V., Eliceiri, K., Tomancak, P., and Cardona, A. (2012) Fiji: An open-source platform for biological-image analysis. *Nat. Methods*. **9**, 676–682
35. Asuni, A. A., Gray, B., Bailey, J., Skipp, P., Perry, V. H., and O'Connor, V. (2014) Analysis of the hippocampal proteome in ME7 prion disease reveals a predominant astrocytic signature and highlights the brain-restricted production of clusterin in chronic neurodegeneration. *J. Biol. Chem.* **289**, 4532–4545

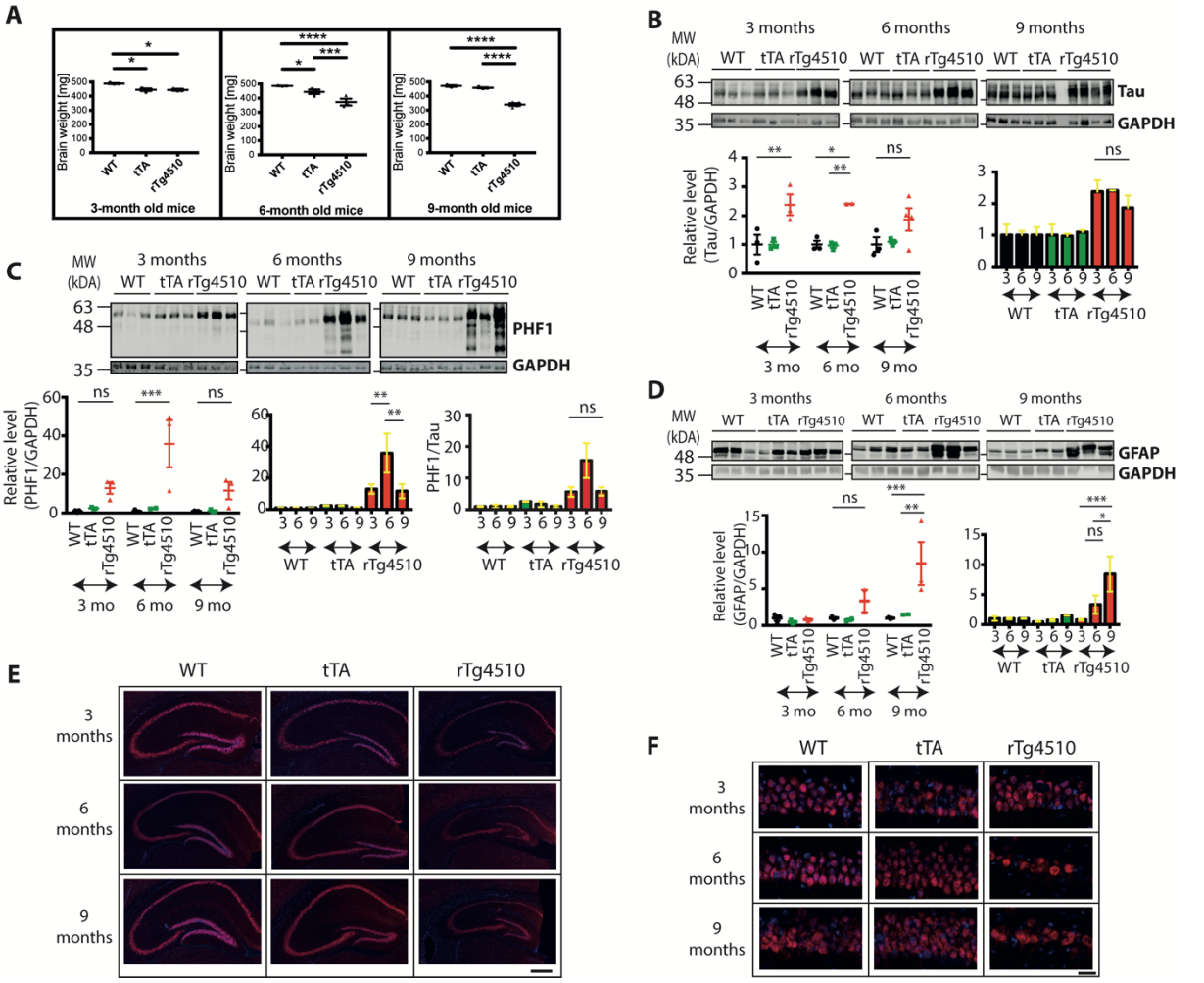

Figure 1. rTg4510 mice can be characterized by progressive pathology. (A) Brain weight changes for 3, 6 and 9-month old WT, tTA and rTg4510 mice. Error bars are SEM; *p<0.05, ***p<0.001, ****p<0.0001. n= 2-4 (B) Western blot showing the total level of tau protein in 3, 6 and 9-month old WT, tTA and rTg4510 mice. The blots were reprobed with GAPDH antibody to illustrate equivalent protein loading. Each lane corresponds to a separate animal. Error bars are SEM; *p<0.05, **p<0.01. (C) Western blot showing the level of phosphorylated tau in 3, 6 and 9-month old WT, tTA and rTg4510 mice. PHF1 antibody directed against Ser396/Ser404 was used. The blots were reprobed with GAPDH antibody to illustrate equivalent protein loading. The level of p-tau was quantified against GAPDH (left and middle panel) and against total tau (right panel). Each lane corresponds to a separate animal. Error bars are SEM; **p<0.01, ***p<0.001. (D) Western blot showing the level of GFAP in 3, 6 and 9-month old WT, tTA and rTg4510 mice. The blots were reprobed with GAPDH antibody to illustrate equivalent protein loading. Each lane corresponds to a separate animal. Error bars are SEM; *p<0.05, **p<0.01, ***p<0.001. (E) Immunohistochemical staining of 3, 6 and 9-month old WT, tTA and rTg4510 mice. NeuN antibody was used to stain the neuronal nuclei (red) and Hoechst stain was used to stain nuclei of all the cell types (blue). The scale bar indicates 500 µm. (F) High resolution images of CA1 region of 3, 6 and 9-month old WT, tTA and rTg4510 mice stained with NeuN antibody. The scale bar indicates 20 µm.

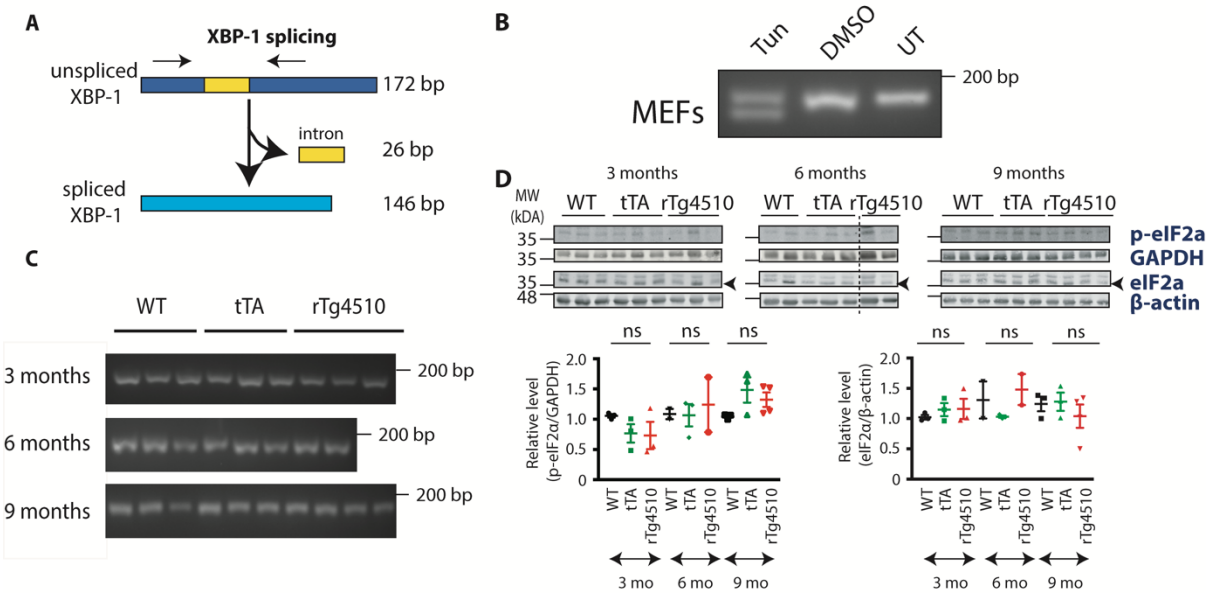

Figure 2. Neither IRE1 nor PERK pathway is activated in rTg4510 animals. (A) Schematic picture illustrating the splicing of XBP-1 gene leading to the formation of a shorter spliced form and 26 base pairs (bp) long intron. The black arrows indicate where the primers bind so that can amplify unspliced and spliced form. (B) cDNA from mouse embryonic fibroblasts (MEFs) treated with tunicamycin (Tun), DMSO (vehicle treatment) or left untreated (UT) was subjected to PCR experiment with XBP-1 primers detecting both, unspliced and spliced, forms of XBP-1. The products were resolved on 2.5% agarose gel. (C) cDNA from 3, 6, 9-month old WT, tTA and rTg4510 mice was subjected to PCR experiment with XBP-1 primers detecting both, unspliced and spliced, forms of XBP-1. The products were resolved on 2.5% agarose gel. n= 2-4 (D) Western blot showing the level of p-eIF2α and total eIF2α protein in the cortex of 3, 6 and 9-month old WT, tTA and rTg4510 mice. The blots were reprobed with GAPDH or actin antibody to illustrate equivalent protein loading. Each lane corresponds to a separate animal. Dashed line indicates splicing of the scan. Error bars are SEM.

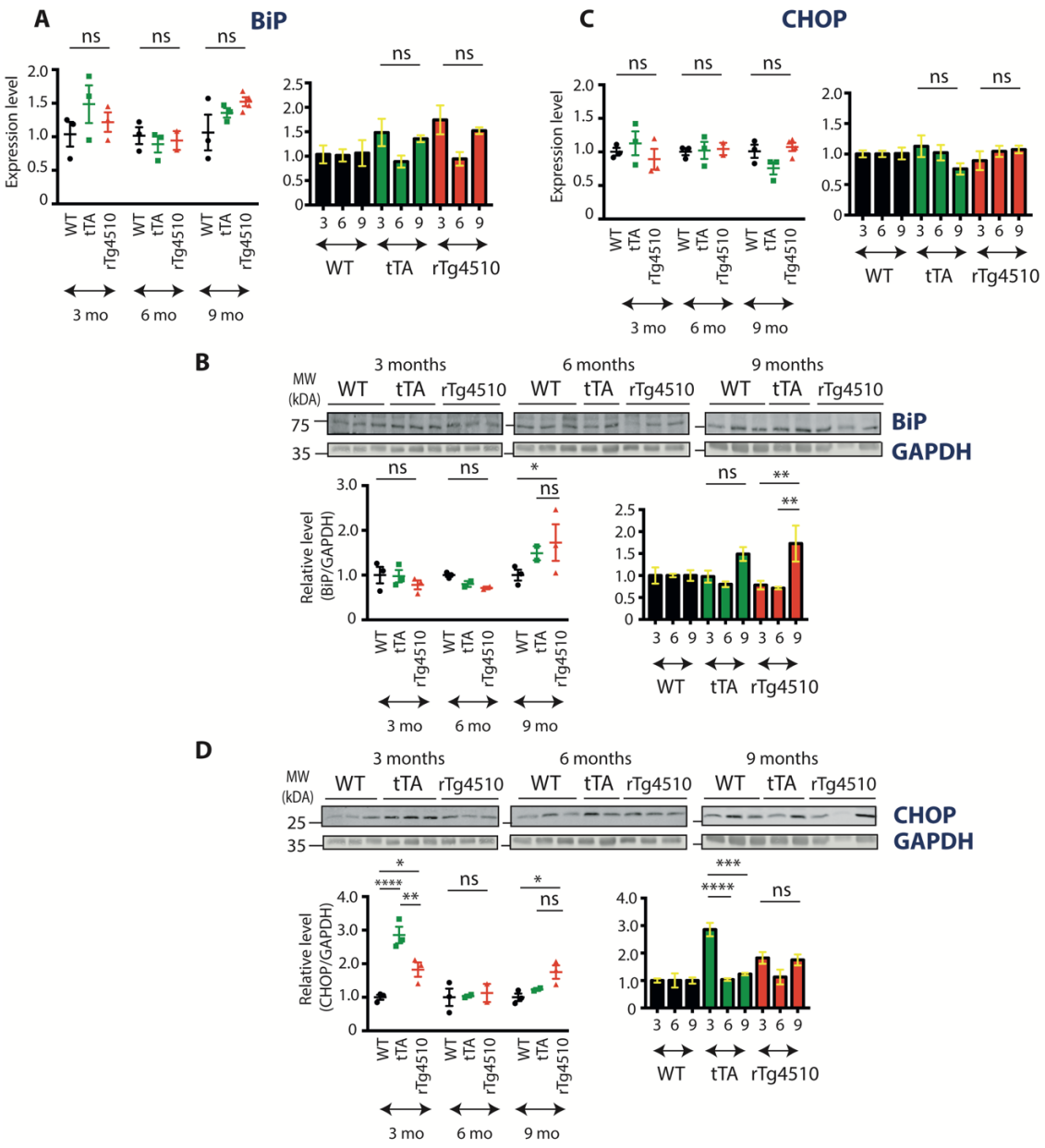

Figure 3. BiP and CHOP expression in rTg4510 animals. (A) qPCR experiment result showing the expression level of BiP transcript in 3, 6 and 9-month old WT, tTA and rTg4510 animals. Error bars are SEM. n= 2-4 (B) Western blot showing the level of BiP protein in 3, 6 and 9-month old WT, tTA and rTg4510 mice. The blots from figure 1D were reprobed with BiP antibodies; the GAPDH signal (also see figure 1D) illustrates equivalent protein loading. Each lane corresponds to a separate animal. Error bars are SEM; *p<0.05, **p<0.01. (C) qPCR experiment result showing the expression level of CHOP transcript in 3, 6 and 9-month old WT, tTA and rTg4510 animals. Error bars are SEM. n= 2-4 (D) Western blot showing the level of CHOP protein in 3, 6 and 9-month old WT, tTA and rTg4510 mice. The blots from figures 1D and 3B were reprobed with CHOP antibodies; GAPDH (also see figures 1D and 3B) illustrates equivalent protein loading. Each lane corresponds to a separate animal. Error bars are SEM; *p<0.05, **p<0.01, ****p<0.0001.

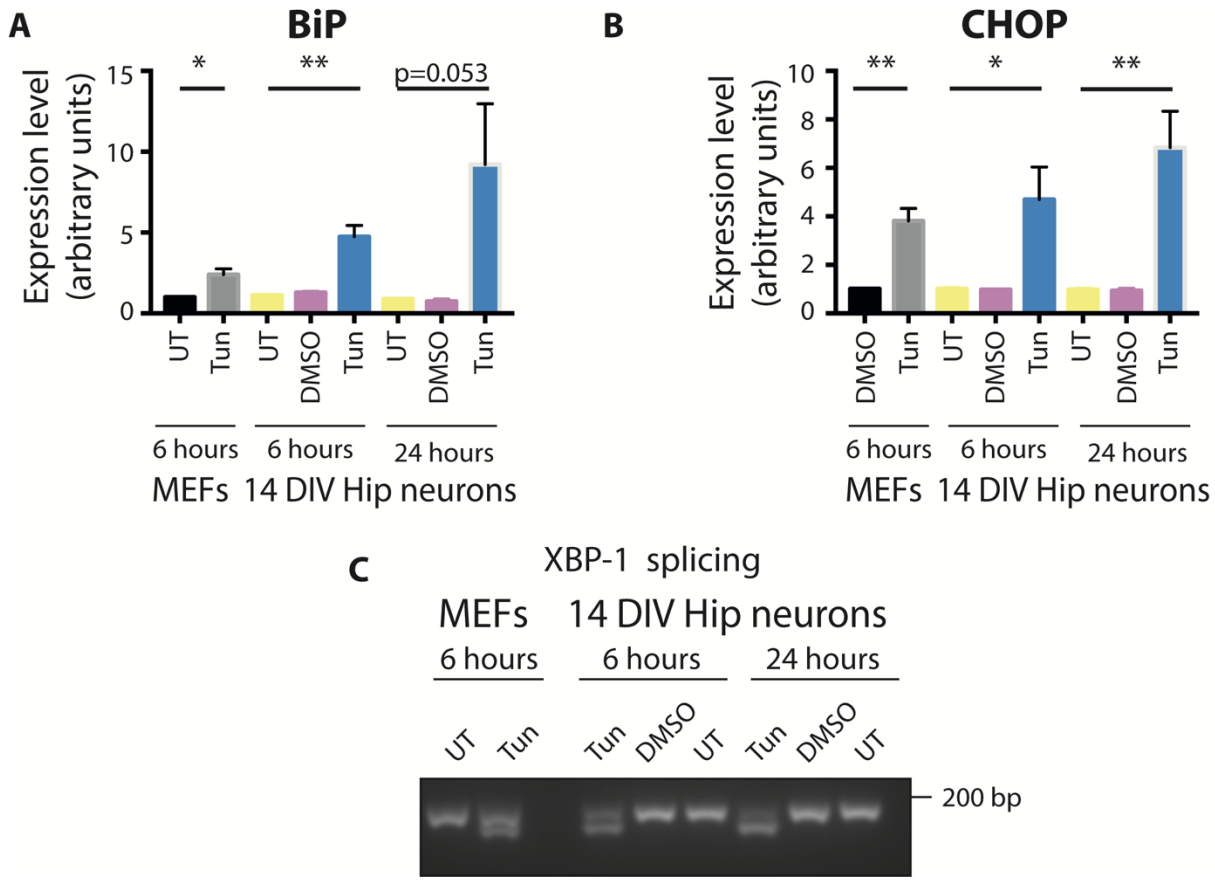

Figure 4. Tunicamycin can induce UPR in primary neurons. (A) Expression level of BiP mRNA in primary neurons treated with tunicamycin, DMSO or left untreated for 6 and 24 hours. MEFs treated with tunicamycin were run alongside as a positive control. The expression level was normalised to eIF4a expression level. Error bars are SEM; *p<0.05, **p<0.01. n= 3 (B) Expression level of CHOP mRNA in primary neurons treated with tunicamycin, DMSO or left untreated for 6 and 24 hours. MEFs treated with tunicamycin were run alongside as a positive control. The expression level was normalised to eIF4a expression level. Error bars are SEM; *p<0.05, **p<0.01. n= 3 (C) RNA was extracted from primary neurons treated with tunicamycin, DMSO or left untreated for 6 and 24 hours and subjected to PCR reaction with primers detecting spliced and unspliced forms of XBP-1. The products were run on the agarose gel. MEFs treated with tunicamycin were run alongside as a positive control.

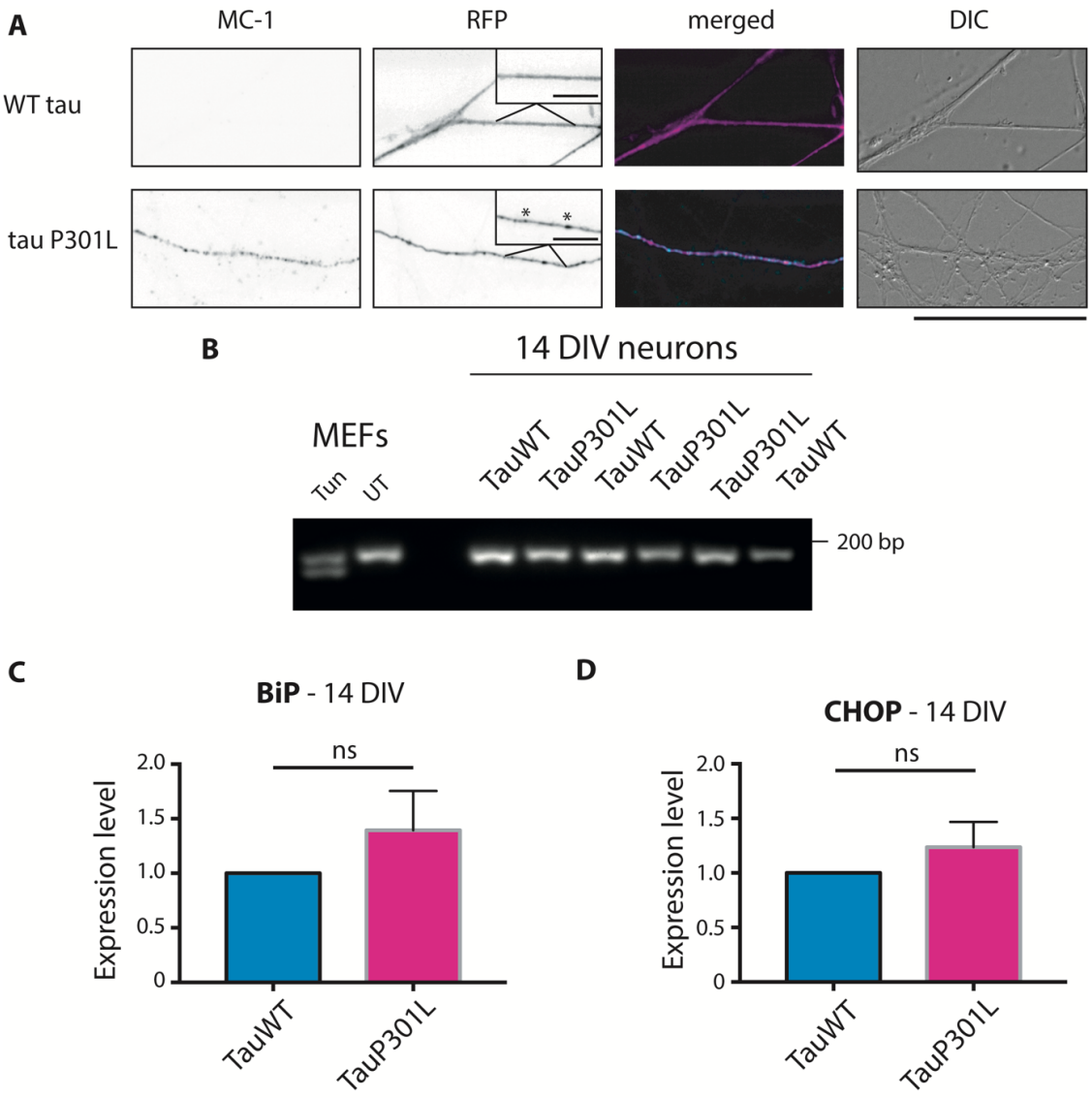

Figure 5. UPR in the primary neurons expressing tauP301L. (A) Images comparing the axons of the neurons expressing tau^{P301L}-RFP and tau^{WT}-RFP, cultured for 14 days in vitro. MC-1 staining in tau^{P301L}-transfected cells suggests the presence of conformationally changed tau. The co-localization of MC-1 staining (cyan) and tau^{P301L}-RFP (magenta) confirms that staining is present only in mutant tau-transfected cells and not in the surrounding untransfected axons. The insets show higher magnification of the axon with the asterisks indicating the aggregates. The scale bar indicates 50 µm. The scale bars for the insets indicate 10 µm. (B) Primary neurons electroporated with tau^{P301L} and tau^{WT} were subjected to PCR experiment with XBP-1 primers and the products were resolved on 2.5% agarose gel. MEFs treated with tunicamycin were run alongside as a positive control. The electroporation efficiency was consistently at 70-80%. n= 3 (C) qPCR experiment result showing the expression level of BiP transcript primary neurons electroporated with tau^{P301L} and tau^{WT}. Expression level was normalised to the expression level of human tau. n= 3 (D) qPCR experiment result showing the expression level of CHOP transcript primary neurons electroporated with tau^{P301L} and tau^{WT}. Expression level was normalised to the expression level of human tau. Error bars are SEM. n= 3.